VOLUME 74, NUMBER 6

JOC Featured Article

March 20, 2009

Solid-State NMR and X-ray Analysis of Structural Transformations in O−H···N Heterosynthons Formed by Hydrogen-Bond-Mediated Molecular Recognition

Mujeeb Khan, Volker Enkelmann, and Gunther Brunklaus*

Max-Planck-Institut für Polymerforschung, Postfach 31 48, D-55021 Mainz, Germany

brunklaus@mpip-mainz.mpg.de

Received December 6, 2008

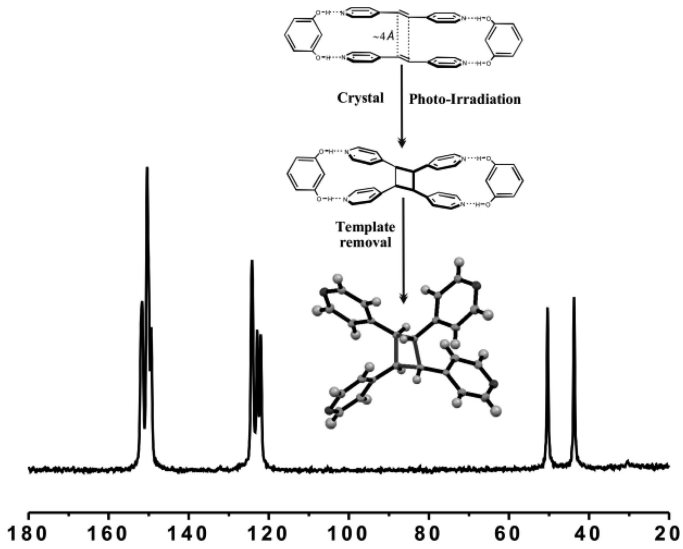

The template-mediated, hydrogen-bond-driven *co-crystallization* of *trans*-1,2-bis(4-pyridyl)ethylene (bpe) and resorcinol together with 1,2-bis(4-pyridyl)ethane (bpet) yielded two new polymorphs of 2(bpe):2(res) and 2(bpet):2(res) *molecular adducts*, thereby exploiting the molecular specificity of resorcinol−pyridine O−H···N recognition in the presence of multiple dipyridines. Comprehensive understanding of the subsequent [2 + 2] photodimerization of the known polymorph of 2(bpe):2(res) complex was obtained by applying single-crystal X-ray analysis and ^{13}C CPMAS solid-state NMR at different levels of conversion, ranging from monomer to the dimer. In addition, removal of the resorcinol template from the 2(bpe):2(res) complex yields a distorted tetrakis(4-pyridyl)cyclobutane, revealing a rather different molecular geometry (orthorhombic, *Pccn* phase). Ambiguous peak splittings and the presence of unexpected resonances in the respective ^{13}C CPMAS NMR spectra have been successfully explained by the joint approach of X-ray analysis and density functional theory (DFT) chemical shift computations.

1. Introduction

Crystal engineering comprises the rational design of functional molecular solids[1−3] that are of fundamental and practical interest to both solid-state and structural chemists on their quest to design organized phases and intermolecular assemblies. Prominent examples are found in the field of organic solid-state photochemistry[4,5] and also include studies on the packing of molecular crystals.[6] Though insights on how intermolecular forces influence the organization of molecules in solids have markedly improved recently,[7] the

10.1021/jo802673f CCC: $40.75 © 2009 American Chemical Society
Published on Web 02/24/2009

design and construction of solids "at will" with predetermined properties (e.g., reactivity, optical) is still rather difficult.[8] Both reactivity and selectivity in most solid-state reactions are constrained by requirements of the host crystal lattice that in ideal situations is held by robust intermolecular interactions like $\pi-\pi$ stackings or hydrogen bonds. Indeed, the directionality and flexibility of the latter have been exploited to allow not only for specific self-assembly[7,9] but also for molecular recognition.[10–12] While the majority of organic solid-state reactions involve the controlled formation of covalent bonds,[12] the concept of *co-crystallization* constitutes an approach to heteromeric products without making or breaking of covalent bonds. Co-crystals may be regarded as peculiar, but inherently rather ill-defined class of structures that facilitate, for example, both an increased pharmaceutical activity of drug compounds and a route to energetic materials.[13] While, in principle, solid-state reactions do not require prior formation of co-crystals and may conveniently proceed under *solvent-free conditions* (e.g., when simply grinding the solid reagents[14]), co-crystallization offers high degrees of stereo- and regiocontrol,[15] respectively.

MacGillivray et al.[16] have enforced topochemical alignment[17] of olefins in the solid state via hydrogen bonds using 1,3-dihydroxybenzene (resorcinol) as a linear template. The 1:1 co-crystallization of resorcinol with *trans*-1,2-bis(4-pyridyl)ethylene (bpe) produced a so-called 0-D complex (forming discrete rings, polymorph **1**),[16] 2(bpe):2(res), with the two C═C bonds oriented parallel and separated by 3.65 Å. This crystal arrangement complies with the well-known topochemical principles[17] and thus, upon broadband UV irradiation, yields the photodimer tetrakis(4-pyridyl)cyclobutane (cf. Scheme 1).

SCHEME 1. Schematic Representation of [2 + 2] Photodimerization of 1:1 Co-crystallization of 2(bpe):2(res)

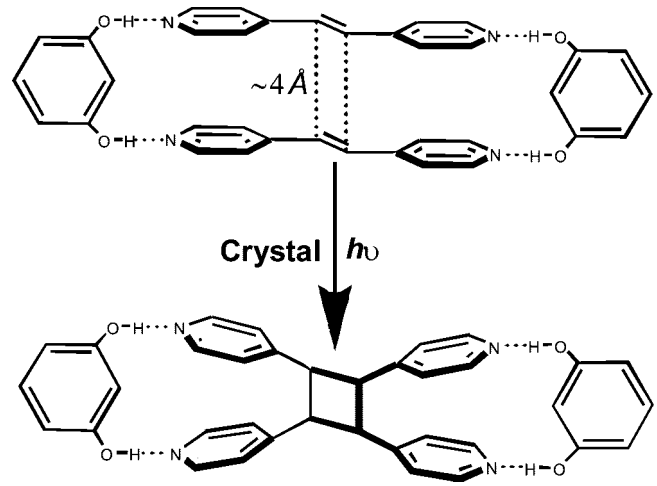

Recently, emphasis had been placed on performing photodimerizations in a single-crystal-to-single-crystal (SCSC) fashion via tail irradiation;[18] that is, *photoactive* crystals were irradiated by (UV) light for which they have rather low absorptivity. Under such selective conditions, the destruction of crystals is avoided and intermediate stages of the photodimerization reaction could be obtained[19] *allowing more detailed insights into solid-state reaction mechanisms.* However, X-ray characterization of amorphous or ill-defined solids lacking long-range translational order as well as localization of lighter atoms (e.g., hydrogen-bonded protons)[20] may be rather demanding even with most sophisticated X-ray diffraction methods.[21] This indeed renders an identification of polymorphs[22] possibly obtained during organic solid-state reactions extremely difficult. The *occurrence of polymorphism*, however, may have far reaching implications on physical properties, thus impacting applications in the pharmaceutical and explosives industries.[23]

Solid-state NMR has been successfully applied to monitor organic solid-state photoreactions.[24−27] Its unique selectivity allowed for the differentiation of chemically distinct sites, including protons,[20] on the basis of the NMR chemical shift,[28] thereby revealing molecular species present in a sample, including product, reactants, possible side products, and polymorphs.[24,27,29] In some cases, however, polymorphs may not yield observably different NMR spectra, for example, if

(1) Desiraju, G. R. *Angew. Chem., Int. Ed.* **2007**, *46*, 8342–8356. (b) Desiraju, G. R. *Angew. Chem., Int. Ed. Engl.* **1995**, *34*, 2311–2327. (c) Desiraju, G. R. *Nat. Mater.* **2002**, *1*, 77–79. (d) Desiraju, G. R. *Nature* **2001**, *412*, 397–400. (e) Desiraju, G. R. *Chem. Commun.* **1997**, *16*, 1474–1482.
(2) Soldatov, D. V.; Terekhova, I. S. *J. Struct. Chem.* **2005**, *46*, S1–S8.
(3) Braga, D. *Chem. Commun.* **2003**, *22*, 2751–2754.
(4) Schmidt, G. M. J.; *Solid State Photochemistry*; Monographs in Modern Chemistry; Ginsburg, D., Ed.; Verlag Chemie: Weinheim, Germany, 1976; Vol. 8.
(5) Ramamurthy, V.; Venkatesan, K. *Chem. Rev.* **1987**, *87*, 433–481. (b) Scheffer, J. R.; Garcia-Garibay, M.; Nalamasu, O. *Org. Photochem.* **1987**, *8*, 249–347. (c) Irie, M.; Kobatake, S.; Horichi, M. *Science* **2001**, *291*, 1769–1772.
(6) Kitaigorodskii, A. I. *Molecular Crystals and Molecules*; Academic Press: New Nork, 1973.
(7) Aekeröy, C. B.; Salmon, D. J. *CrystEngComm.* **2005**, *72*, 439–448.
(8) Scheffer, J. R.; Xia, W. *Top. Curr. Chem.* **2005**, *254*, 233–262.
(9) MacGillivray, L. R. *J. Org. Chem.* **2008**, *73*, 3311–3317. (b) MacGillivray, L. R.; Papaefstathiou, G. S.; Friscic, T.; Hamilton, D.; Bucar, D. K.; Chu, Q.; Varshney, D. B.; Georgiev, I. G. *Acc. Chem. Res.* **2008**, *41*, 280–291. (c) Papaefstathiou, G. S.; MacGillivray, L. R. *Org. Lett.* **2001**, *3*, 3835–3838. (d) Friscic, T.; MacGillivray, L. R. *Mol. Cryst. Liq. Cryst.* **2006**, *456*, 155–162. (e) The relatively low density of the 2(bpet):2(res) polymorph reported by MacGillivray et al. in our opinion indicates that it is the less stable form of 2(bpet)2(res) in the chain form compared to the polymorph obtained during this study.
(10) Xiao, J.; Yang, M.; Lauher, J. W.; Flower, F. W. *Angew. Chem., Int. Ed.* **2000**, *39*, 2132–2135. (b) Curtis, S. M.; Le, N.; Flower, F. W.; Lauher, J. W. *Cryst. Growth Des.* **2005**, *5*, 2313–2321. (c) Fowler, F. W.; Lauher, J. W. *J. Phys. Org. Chem.* **2000**, *13*, 850–857.
(11) Brunklaus, G.; Koch, A.; Sebastiani, D.; Spiess, H. W. *Phys. Chem. Chem. Phys.* **2007**, *9*, 4545–4551.
(12) Braga, D.; Grepioni, F. *Angew. Chem., Int. Ed.* **2004**, *43*, 4002–4011.
(13) Foerter-Barth, U.; Herrmann, M.; Kempa, P. B.; Teipel, U. *Chem.-Ing.-Tech.* **2007**, *79*, 1410.
(14) Roberts, B. A.; Cave, G. W. V.; Raston, C. L.; Scott, J. L. *Green Chem.* **2001**, *3*, 280–284.
(15) Feldman, K. S.; Campbell, R. F. *J. Org. Chem.* **1995**, *60*, 1924–1925.
(16) MacGillivray, L. R.; Reid, J. L.; Ripmeester, J. *J. Am. Chem. Soc.* **2000**, *122*, 7817–7818.
(17) Schmidt, G. M. J. *Pure Appl. Chem.* **1971**, *27*, 647–678.
(18) Abdelmoty, I.; Buchholz, V.; Di, L.; Enkelmann, V.; Wegner, G.; Foxman, B. M. *Cryst. Growth Des.* **2005**, *5*, 2210–2217.
(19) Enkelmann, V.; Wegner, G.; Novak, K. *J. Am. Chem. Soc.* **1993**, *115*, 10390–10391. (b) Novak, K.; Enkelmann, V.; Wegner, G. *Angew. Chem., Int. Ed. Engl.* **1993**, *32*, 1614–1616.
(20) Brown, S. P. *Prog. Nucl. Magn. Reson.* **2007**, *50*, 199–251. (b) Brown, S. P.; Spiess, H. W. *Chem. Rev.* **2001**, *101*, 4125–4155. (c) Harris, R. K. *Solid State Sci.* **2004**, *6*, 1025–1037.
(21) Harris, K. D. M.; Cheung, E. Y. *Chem. Soc. Rev.* **2004**, *33*, 526–538.
(22) Dunitz, J. D.; Bernstein, J. *Acc. Chem. Res.* **1995**, *28*, 193–200.
(23) Bowes, K. F.; Clark, I. P.; Cole, J. M.; Gourlay, M.; Griffin, A. M. E.; Mahon, M. F.; Ooi, L.; Parker, A. W.; Raithby, P. R.; Sparkes, H. A.; Towrie, M. *CrystEngComm.* **2005**, *7*, 269–275.
(24) Khan, M.; Brunklaus, G.; Enkelmann, V.; Spiess, H. W. *J. Am. Chem. Soc.* **2008**, *130*, 1741–1748.
(25) Stitchell, S. G.; Harris, K. D. M.; Aliev, A. E. *Struct. Chem.* **1994**, *5*, 327–333. (b) Harris, K. D. M.; Thomas, J. M. *J. Solid State Chem.* **1991**, *94*, 197–205.
(26) Hilgeroth, A.; Hempel, G.; Baumeister, U.; Reichert, D. *Solid Stat. Nucl. Magn. Reson.* **1999**, *13*, 231–243.
(27) Bertmer, M.; Nieuwendaal, R. C.; Barnes, A. B.; Hayes, S. E. *J. Phys. Chem. B* **2006**, *110*, 6270–6273.
(28) Harris, R. K. *Solid State Sci.* **2004**, *6*, 1025–1037.
(29) Harris, R. K. *Analyst* **2006**, *131*, 351–373.

small chemical shift differences are obscured by moderately large line widths even under magic-angle spinning conditions.[30] Hence, the combined approach of solid-state NMR and (single-crystal) X-ray analysis provides in-depth information about the topochemical nature of solid-state reactions as well as structural changes occurring at the molecular level during the reaction.[24,27]

In this contribution, we present the results of a detailed solid-state NMR analysis of both the hydrogen-bond-driven co-crystallization and subsequent [2 + 2] photodimerization of *trans*-1,2-bis(4-pyridyl)ethylene with resorcinol (polymorph **1**). Moreover, in order to explore the *molecular specificity* of the resorcinol−pyridine recognition, bpe has been co-crystallized together with resorcinol in the presence of the rather *similar* hydrogen-bonding acceptor 1,2-bis(4-pyridyl)ethane (bpet). The latter compound is selected as it is nearly *isostructural* to bpe, except the former has a double bond connecting two pyridyl rings instead of a single bond. Structural changes occurring during this reaction were also monitored via single-crystal X-ray analysis, where possible, thus establishing the nature and reaction pathways of this supramolecular heterosynthon. To further explore structural impacts of crystal packing or template effects, we subsequently removed resorcinol from the dimeric assembly via solvent extraction. All structures are compared and discussed with respect to the recorded ^{13}C CPMAS spectra.

2. Results and Discussion

Reactions in the solid state mostly occur with a minimum amount of molecular motion. In other words, the environment in the solid state is flexible enough to allow for atoms to move and react, but yet is sufficiently rigid to enable reactions to proceed with a remarkable stereocontrol. In order to gain comprehensive understanding of the template-mediated organic solid-state reaction of the 2(bpe):2(res) supramolecular heterosynthon, a joint approach of solid-state NMR and X-ray analysis has been applied. Prior to deriving mechanistical details of the [2 + 2] photodimerization of 2(bpe):2(res) heterosynthon, we will first consider the structure of both the template (resorcinol) and the substrate (bpe) that are involved in the photoreaction and then proceed to analyze the molecular specificity of the O−H···N heterosynthon.

Structure of Resorcinol. Figure 1 displays the recorded ^{13}C CPMAS NMR spectra of both resorcinol and *trans*-1,2-bis(4-pyridyl)ethylene (the spectral assignment is given in Table 1). While the ^{13}C solution NMR spectrum of resorcinol (cf. Supporting Information) exhibits four resonances reflecting its molecular structure, the solid-state ^{13}C CPMAS NMR spectrum (Figure 1a) of resorcinol displays six different carbon signals. The latter is readily explained by the crystal structure of resorcinol[31] containing more than one molecule of resorcinol in the corresponding unit cell, which is frequently found for molecular crystals.[28,32] The asymmetric unit of the resorcinol crystal structure is comprised of *one* resorcinol molecule that occupies a general position of symmetry in the unit cell, rendering the carbons (C1,C3) and (C4,C6) *diastereotopic*.

The molecular packing of resorcinol within the orthorhombic crystals (space group $Pna2_1$ (No. 33), $Z = 4$, CSD code: RESORA13; cf. Figure 2)[31] comprises *four* resorcinols where each

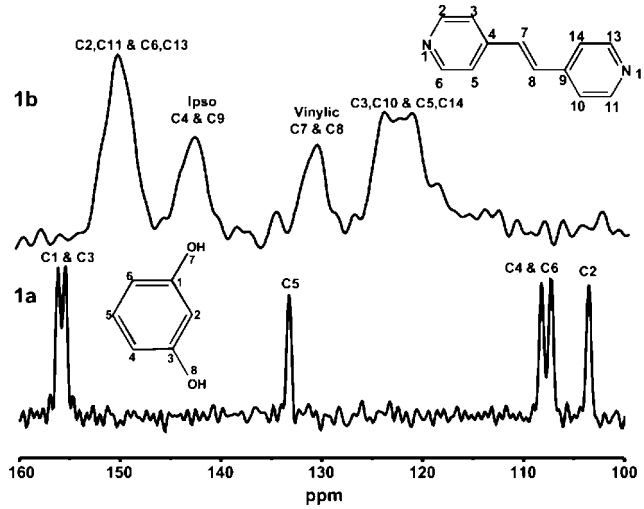

FIGURE 1. Solid-state ^{13}C CPMAS of (a) 1,3-dihydroxybenzene (resorcinol), (b) *trans*-1,2-bis(4-pyridyl)ethylene, where chemical shift dispersion is mainly responsible for the broad lines in the spectrum of **1b**.

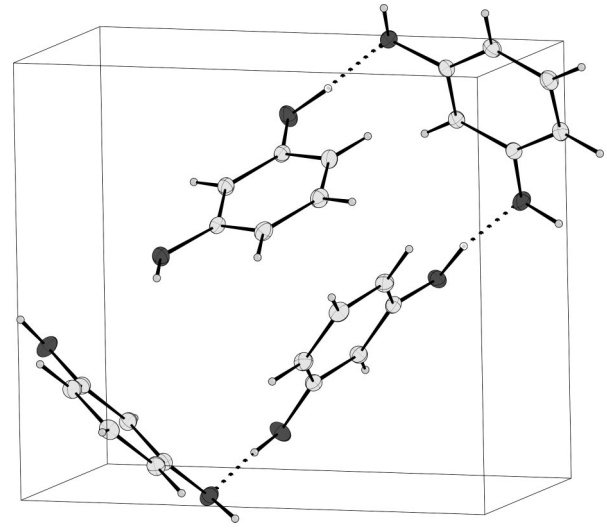

FIGURE 2. Molecular packing of 1,3-dihydroxybenzene (resorcinol). Single-crystal data were taken from the Cambridge Structural Database (CSD code: RESORA13).[31b] (The dotted lines represent H-bonding among the OH groups of resorcinol.)

molecule has two different neighbors that are linked via different hydrogen bonds. Thus, in comparison to solution ^{13}C NMR, additional signals observed in the corresponding solid-state ^{13}C CPMAS NMR spectrum of resorcinol (cf. Figure 1a) are clearly attributed to different magnetic environments of the carbons in each molecule that is packed in the unit cell. This was further confirmed with DFT ^{13}C chemical shift computations using the crystal structure as-obtained from the literature (cf. Figure 3).

Structure of *trans*-1,2-Bis(4-pyridyl)ethylene (bpe). The solid-state ^{13}C CPMAS spectrum of bpe (cf. Figure 1b) shows at least five rather broad resonances (there are *two* signals at 150 ppm that are unresolved) reflecting molecular packing effects as previously observed for resorcinol. Notably, bpe is not located on a center of symmetry but rather occupies a general position in the unit cell. Consequently, the asymmetric unit of bpe consists of *one* bpe molecule rendering all 12 carbon atoms of a bpe molecule inequivalent. However, the ^{13}C chemical shift differences are apparently rather small and not fully resolvable in the respective ^{13}C CPMAS spectrum. Further contributions

(30) Tam, C. N.; Cowan, J. A.; Schultz, A. J.; Young, V. G.; Trouw, F. R., Jr.; Sykes, A. G. *J. Phys. Chem. B* **2003**, *107*, 7601–7606.

(31) Robertson, J. M. *Proc. R. Soc. London, Ser. A* **1936**, *157*, 79–99. (b) Bacon, G. E.; Jude, R. J. *Z. Kristallogr.* **1973**, *19*, 138.

(32) Masuda, K.; Tabata, S.; Kono, H.; Sakata, Y.; Hayase, T.; Yonemochi, E.; Tarada, K. *Int. J. Pharm.* **2006**, *318*, 146–153.

TABLE 1. ^{13}C CPMAS NMR Resonance Assignments for Resorcinol, *trans*-1,2-Bis(4-pyridyl)ethylene, 2(bpe):2(res) Monomer, 2(bpe):2(res) Recrystallized Dimer (Monoclinic, $P2_1/n$ Phase), and Tetrakis(4-pyridyl)cyclobutane, Based on DFT ^{13}C Chemical Shift Computations

sample	experimental δ (ppm)	assignment
1,3-dihydroxybenzene (resorcinol)	106.3	center carbon (C2)
	107.2	next to edge carbon (C4)
	108.2	next to edge carbon (C6)
	133.2	edge carbon (C5)
	155.3	next to OH carbon (C1)
	156.1	next to OH carbon (C3)
trans-1,2-bis(4-pyridyl)ethylene (bpe)	121.1	next to ipso carbon (C5,C14)
	123.9	next to ipso carbon (C3,C10)
	130.4	vinylic carbons (C7,C8)
	142.4	ipso carbons (C4,C9)
	150.0	next to N carbons (C2,C11 and C6,C13)
2(bpe):2(res) monomer (prior to irradiation)	103.2	res center carbons (C30,C38)
	106.7	res carbons (C32,C34,40,42)
	120.4	bpe carbons (C3,C10,C17,C24)
	125.0	bpe carbons (C5,C14,C19,C28)
	128.8	vinylic carbons (C7,C8,C21,C22)
	130.7	res edge carbons (C33,C41)
	143.7	ipso carbons (C4,C9,C18,C23)
	148.6−150.5	bpe carbons (C2,C6,C11,C13 and C16,C20,C25,C27)
	162.7	res carbons (C29,C31,C37,C39)
2(bpe):2(res) recrystallized dimer monoclinic $P21/n$ phase	42.8	cyclobutane carbons (C7,C8,C9,C10)
	100.9	res carbons (C30,C38)
	106.8	res carbons (C32,C34,C40,C42)
	125.1−126.5	bpe carbons next to ipso (C3,C5,C24,C28,C12,C16,C22,C18)
	130.5	res carbons (C33,C41)
	147.4	bpe carbons next to N (C2,C6,C13,C15,C19,C21,C25,C27)
	151.4	ipso carbons (C4,C11,C17,C23)
	161.3	res carbons (C29,C31,C37,C39)
tetrakis(4-pyridyl)cyclobutane (without resorcinol)	43.7	cyclobutane carbons (C20,C24)
	50.3	cyclobutane carbons (C6,C10)
	122.0	next to ipso carbons (C5,C7)
	122.8	next to ipso carbons(C23,C28)
	124.9	next to ipso carbons (C9,C14,C19,C21)
	149.4	ipso carbons (C17,C18)
	150.3	ipso and next to N carbons (C3,C4 and C11,C12,C22,C27)
	151.6	carbons next to N (C8,C13,C25,C26)

to the experimental line broadening (cf. Figure 1b) are most likely due to different neighbors of bpe reflecting different magnetic environments (cf. Figure 4).

DFT ^{13}C chemical shift computations based on an optimized bpe molecule extracted from the crystal structure (Figure 5, CSD code: AZSTBB[16]) notably predict signal splittings of 7 ppm for carbons (C3,C10 and C5,C14) neighboring ipso carbon, which are quite similar to the experimentally observed splittings (∼4 ppm). Moreover, the smaller computed peak splitting (1.4 pm) of carbons (C2,C11 and C6,C13) next to nitrogen is in good agreement with the experimental ^{13}C CPMAS NMR spectrum (cf. Figure 1b), where two signals have merged at 150 ppm, yielding a rather broad signal. The unlikely broad signals in the ^{13}C CPMAS NMR spectrum of bpe have been reproduced several times and were also found in respective fast

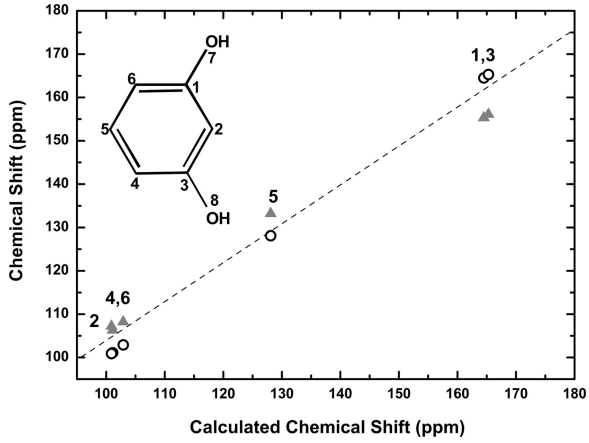

FIGURE 3. Plot of ^{13}C chemical shifts for 1,3-dihydroxybenzene (resorcinol). Open circles represent the computed, and triangles the experimentally observed ^{13}C chemical shifts with respect to the calculated values (the dashed line is a guide to eye). The computed ^{13}C shifts are based on the resorcinol unit cell ($Z = 4$). Computed signal splittings of both C1,C3 and C4,C6 amount to ∼1.5 ppm as observed experimentally (∼1 ppm). The agreement of computed ^{13}C chemical shifts with experimental data is good in the range of ±5 ppm, except for the carbons attached to the hydroxyl group where the difference is ∼9 ppm.

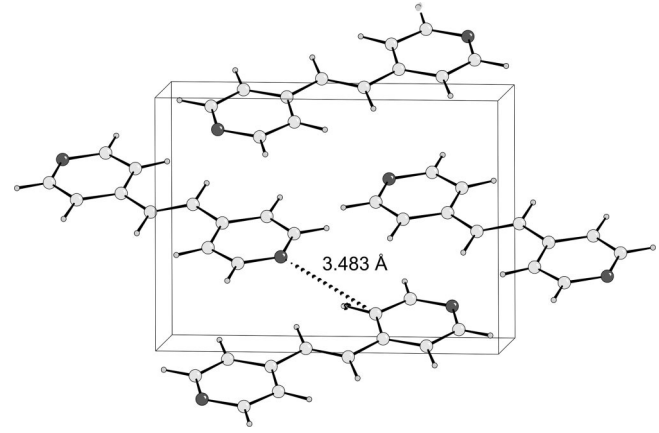

FIGURE 4. Molecular packing of *trans*-1,2-bis(4-pyridyl)ethylene (bpe). Single-crystal data was taken from the Cambridge Structural Database (CSD code: AZSTBB).[16] (The dotted line represents the next nearest neighbor of bpe molecule.)

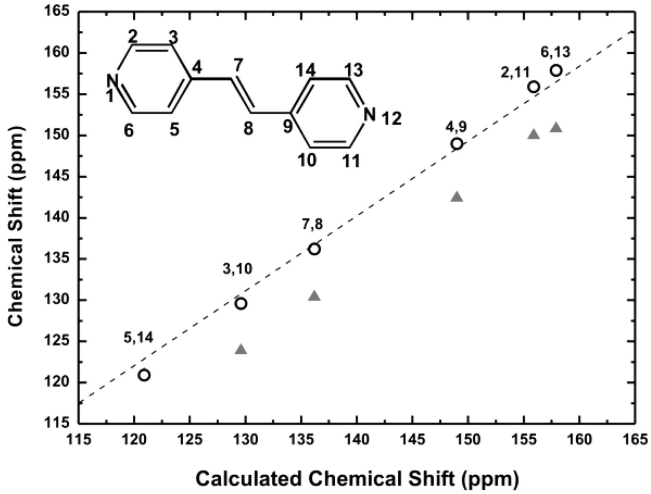

FIGURE 5. Plot of ^{13}C chemical shifts for *trans*-1,2-bis(4-pyridyl)-ethylene (bpe). Open circles represent the computed, and triangles the experimentally observed ^{13}C chemical shifts with respect to the calculated values (the dashed line is a guide to eye). The DFT computed ^{13}C shifts are based on an optimized bpe structure.

MAS proton NMR spectra (data not shown). For perfectly well-arranged (e.g., highly crystalline) solids, severe linebroading in proton MAS spectra stems solely from homonuclear dipolar couplings among abundant protons. In that case, high-resolution proton MAS NMR spectra can, in principle, be obtained using so-called homonuclear dipolar decoupling sequences like windowed phase-modulated Lee-Goldburg (wPMLG)[33] or windowed DUMBO-1[34] that also constitute the key part of high-resolution proton double-quantum spectra (DQ-CRAMPS[35]). Since this approach did *not* yield substantial line narrowing, the experimental line widths were attributed to heterogeneous broadening due to ^{13}C chemical shift dispersion. This implies a rather ill-defined local ordering or poor crystallinity of the bulk NMR sample in contrast to the single crystal used for X-ray analysis, as recently reported for an enolizable chromophore.[36]

Molecular Specificity of O−H···N Heterosynthon. It is known that bpe does not exhibit proper packing (or merely does not crystallize in a form) that is required for solid-state dimerization. In the 2(bpe):2(res) 0-D complex (polymorph **1**, ring form), however, the double bonds are in *parallel* position suitable for a homogeneous [2 + 2] photodimerization.[16] Crystals obtained at *intermediate* stages of the dimerization are referred to as substitutional mixed crystals[19] (which are those where monomer and dimer molecules statistically occupy the same lattice sites) that, in principle, provide detailed insights into atomic level changes occurring during the respective topochemical reaction.

Owing to the possibility of bond rotation about the C−O bond, resorcinols may consist of three different possible conformations of hydroxyl groups with respect to the phenyl ring (cf. Figure 6): *syn-syn*, *anti-anti*, and *syn-anti*.[9d] In order to achieve the required parallel arrangement of bpe for photodimerization, the OH group must adopt *syn-syn* conformation

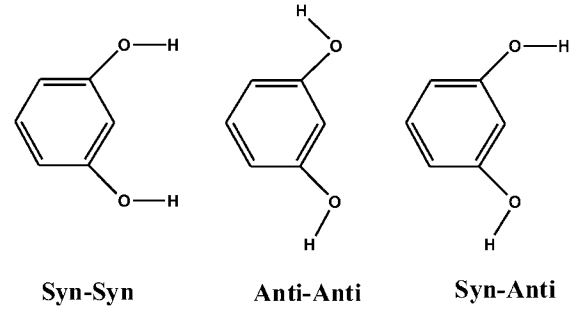

FIGURE 6. Three different possible hydroxyl conformations of resorcinol with respect to the phenyl ring.[9d]

(cf. Scheme 1) as observed in the case of 2(bpe):2(res), where resorcinol is co-crystallized with bpe adopting a ring form (polymorph **1**, triclinic, $P\bar{1}$).

Notably, via co-crystallization of bpe with resorcinol in the presence of saturated dipyridine 1,2-bis(4-pyridyl)ethane (bpet) (which has been selected as it closely resembles bpe) in equimolar ratio (0.5:0.5:1) by slow evaporation in acetone at room temperature, two types of *crystals* were obtained. These crystals could be easily distinguished by their appearance (colorless needles crystallizing first and yellow prisms forming at later stages of the crystallization). The colorless needle-like crystals represent the 2(bpet):2(res) molecular adduct in the chain form (monoclinic, $P2_1/n$ phase), which is identical to the co-crystals previously observed[37] under rather similar crystallization conditions (in acetone) upon co-crystallization of bpet and resorcinol. From now onward, the needle-like crystals are referred to as polymorph **2** of the 2(bpet):2(res) complex (^1H NMR is provided in Supporting Information). In addition, MacGillivray et al. have independently identified another polymorph of 2(bpet):2(res) molecular *adduct* in the chain form (polymorph **1**, triclinic, $P\bar{1}$ phase) applying different crystallization conditions (slow evaporation of acetonitrile; cf. Table 2).[9c,e]

In addition, the yellow prism-shaped crystals were identified as a different polymorph of the 2(bpe):2(res) molecular adduct in the chain form (polymorph **2**, monoclinic, $P2_1/n$ phase). Both structures (polymorph **2** of 2(bpe):2(res) and polymorph **2** of 2(bpet):2(res) in the chain forms) are isostructural (cf. Figure 7) and consist of extended hydrogen-bonded chains with similar lattice parameters (Table 2). Thus, it is rather clear that the new polymorph of 2(bpe):2(res) in the chain form (polymorph **2**) is not suitable for photodimerization. Indeed, fractionation into different crystals that has been observed during the multicomponent co-crystallization from acetone clearly indicates that at least under these conditions the complex formation of resorcinol with bpe and bpet is specific, thus emphasizing the molecular specificity of the resorcinol−pyridine (O−H···N) recognition.

New Polymorph of 2(bpe):2(res) Monomer. Apparently, the new polymorph of monomer 2(bpe):2(res) in chain from polymorph **2** is relatively less stable than the reported ring form, as it has been kinetically driven in the presence of bpet. The latter presumably provides nucleation for the crystallization, as bpet indeed adopts a chain conformation upon crystallization with resorcinol in acetone as described above. Desiraju has

(33) Leskes, M.; Madhu, P. K.; Vega, S. *J. Chem. Phys.* **2008**, *128*, 052309/1–052309/11.

(34) Lesage, A.; Sakellariou, D.; Hediger, S.; Elena, B.; Charmont, P.; Steuernagel, S.; Emsley, L. *J. Magn. Reson.* **2003**, *163*, 105–113.

(35) Brown, S. P.; Lesage, A.; Elena, B.; Emsley, L. *J. Am. Chem. Soc.* **2004**, *126*, 13230–13231.

(36) Bolz, I.; Moon, C.; Enkelmann, V.; Brunklaus, G.; Spange, S. *J. Org. Chem.* **2008**, *73*, 4783–4793.

(37) Khan, M. Application of the Complex Formation between Resorcinols and Pyridines in Crystal Engineering: Control of Distance and Orientation of Photoreactive Molecules. M.S. Thesis, Johannes Gutenberg University, Mainz, Germany, 2005.

(38) Khan, M.; Enkelmann, V.; Brunklaus, G. *CrystEngComm.* **2009**, in press.

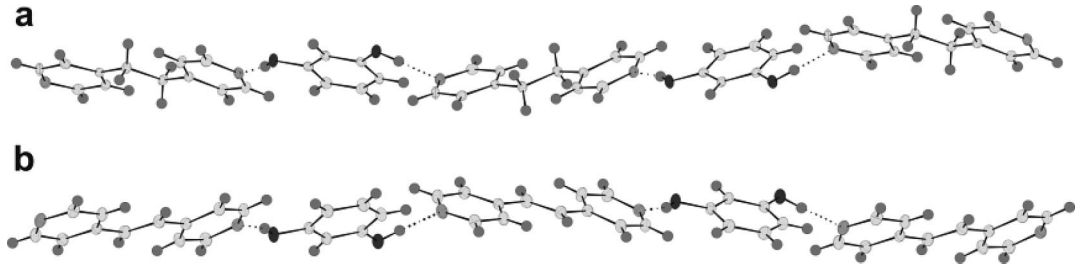

FIGURE 7. (a) Chain conformation of 1,2-bis(4-pyridyl)ethane (bpet) in the compound 2(bpet):2(res) and (b) chain conformation of *trans*-1,2-bis(4-pyridyl)ethylene (bpe) in the compound 2(bpe):2(res). Both monomer adducts crystallize with almost identical lattice parameters.

TABLE 2. Lattice Parameters of Both the Polymorphs of 2(bpe):2(res) Monomer Adduct (Both Chain and Ring Forms), Two Polymorphs of 2(bpet):2(res) (Triclinic $P\bar{1}$ and Monoclinic $P2_1/n$), and Both Dimer Polymorphs (As-Dimerized $P\bar{1}$ Phase and Recrystallized $P2_1/n$ Phase)

lattice parameters	2(bpe):2(res) ring form[16] polymorph **1**	2(bpe):2(res) chain form polymorph **2**	2(bpet):2(res) chain form polymorph **2**	2(bpet):2(res) chain form[9c] polymorph **1**	2(bpe):2(res) as-dimerized dimer (42%)[38]	2(bpe):2(res) recrystallized dimer[16]
a (Å)	8.070 (1)	10.1485 (4)	10.1927 (5)	7.707 (2)	7.7682 (1)	11.367 (1)
b (Å)	9.832 (1)	7.1265 (3)	7.1610 (9)	9.1462 (2)	9.7938 (1)	9.749 (1)
c (Å)	10.876 (1)	20.0717 (6)	20.2559 (8)	11.804 (2)	11.0478 (1)	14.273 (1)
α	73.119 (1)°	90°	90°	87.94 (3)°	94.4493 (1)°	90°
β	72.563 (1)°	94.6837 (21)°	94.1624 (21)°	86.55 (3)°	104.8507 (1)°	111.668 (15)°
γ	66.184 (1)°	90°	90°	71.33 (3)°	111.4950 (1)°	90°
V (Å^3)	738.868	1446.8	1474.6	786.8 (3)	742.068	1469.93
space group	$P\bar{1}$	$P2_1/n$	$P2_1/n$	$P\bar{1}$	$P\bar{1}$	$P2_1/n$

previously suggested[39] that kinetically favored crystals grow faster, but the resulting crystals are less stable since the activation energy barrier to that state is lower. In contrast, thermodynamically favored crystals should take a longer time to form as the activation energy barrier is much higher, but the resulting structure is more stable. Indeed, this has been demonstrated by DSC experiments (not shown here) where the melting temperatures of the stable (ring) and metastable (chain) forms differed by ∼15 °C (215 and 200 °C, respectively).

Structure of 2(bpe):2(res) Monomer. As stated earlier, co-crystallization of resorcinol and bpe in 1:1 ratio yields a 0-D complex of 2(bpe):2(res), where four hydroxyl groups of two resorcinol molecules hold two bpe molecules (ring form, triclinic, $P\bar{1}$) with relatively strong hydrogen bonds forcing them to stack parallel to each other. The corresponding ^{13}C CPMAS NMR spectrum of 2(bpe):2(res) displays well-resolved peaks (Figure 8a), allowing one to distinguish individual signals due to resorcinol and bpe. All signals of resorcinol in the complex 2(bpe):2(res) appear 2−3 ppm downfield shifted compared to pure resorcinol, except for carbons C1 and C3 next to hydroxyl groups that are downfield shifted from ∼156 to 162 ppm due to hydrogen bonding to the nitrogen of the pyridyl rings. Notably, signal splittings corresponding to the carbons neighboring hydroxyl group (C1, C3) and carbons that are next to the peripheral carbon (C4, C6) in resorcinol (cf. Figure 1a) have vanished, indicating changes of the hydrogen bonding pattern.

However, signal splittings corresponding to bpe are more pronounced in the monomer complex 2(bpe):2(res), particularly for signals assigned to the carbons (C3,C10 and C5,C14) next to ipso carbon of bpe which has further increased from 3 ppm in the pure form to about 5 ppm and appeared as two different signals at about 120 and 125 ppm in the solid-state spectrum of 2(bpe):2(res) (cf. Figure 8a). Moreover, the signal at ∼150 ppm corresponding to carbons (C2,C11 and C6,C13) next to nitrogen of the bpe molecule has split unlike in the original bpe ^{13}C CPMAS NMR spectrum where it was unresolved (cf. Figure 1b). Remaining signals at ∼143 and 128 ppm can be assigned to ipso (C4,C9) and vinylic (C7,C8) carbons, respectively. Indeed, the observed signal splittings reflect the molecular packing of the 0-D monomer complex 2(bpe):2(res). Two adjacent bpe molecules in the single block of 2(bpe):2(res) do not lie exactly parallel to each other but are slightly inclined due to which the arms of the hydrogen bonds between the hydroxyl group of resorcinol and the nitrogen of the pyridyl rings are not coplanar (cf. Figure 9). In order to account for solid-state packing effects, DFT ^{13}C chemical shift computations were performed on an optimized monomer 2(bpe):2(res) complex where the computed ^{13}C chemical shifts fit well with experimental data (the agreement is good in the range of ±5 ppm), including peak splittings (cf. Figure 10).

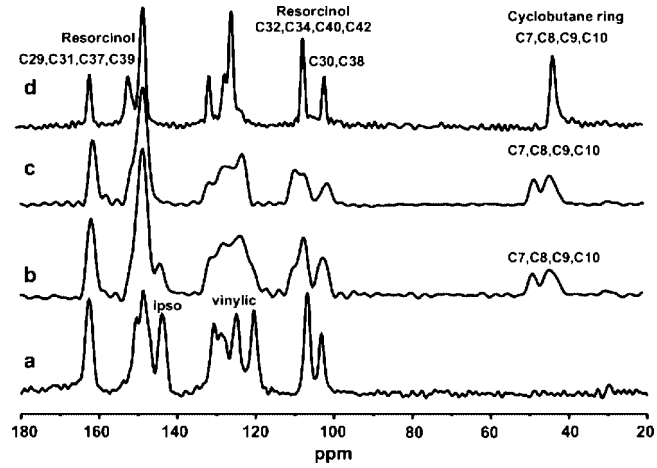

FIGURE 8. Solid-state ^{13}C CPMAS spectra ranging from monomer to dimer: (a) 1:1 co-crystallized 2(bpe):2(res) monomer prior to irradiation; (b) ∼50% converted mixture; (c) 100% converted *as-dimerized* metastable dimer prior to recrystallization, which consists of triclinic $P\bar{1}$ space group (the absence of an ipso carbon signal at ∼140 ppm in 6c is a clear indication of complete conversion); (d) 100% converted recrystallized stable dimer consisting of monoclinic $P2_1/n$ space group.

(39) Desiraju, G. R. *Nat. Mater.* **2002**, *1*, 77–79.

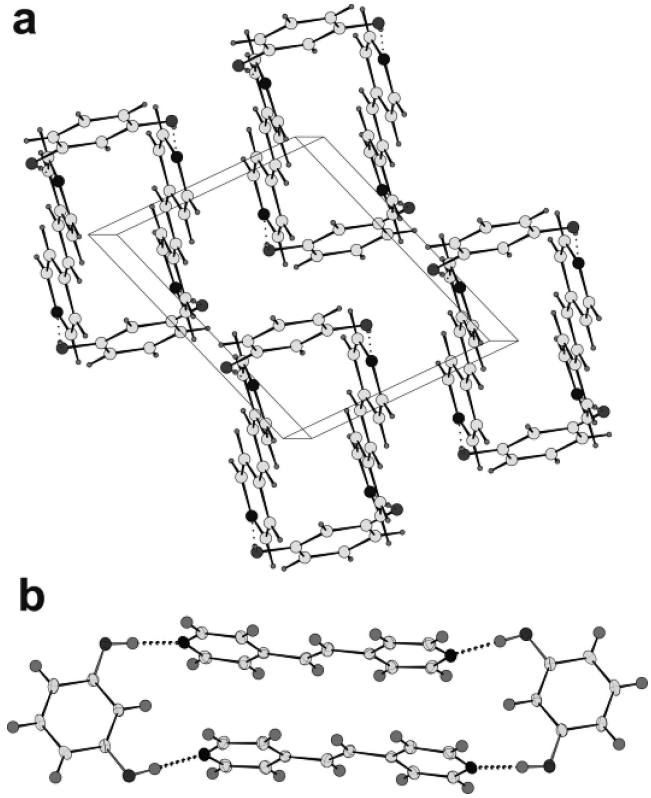

FIGURE 9. (a) Molecular packing of the 1:1 co-crystallized 2(bpe):2(res) monomer complex prior to irradiation; (b) single block of 2(bpe):2(res) where two bpe molecules do *not* lie parallel to each other but are slightly inclined. Single-crystal data was taken from the Cambridge Structural Database (CSD code: ABEKLIN).[16]

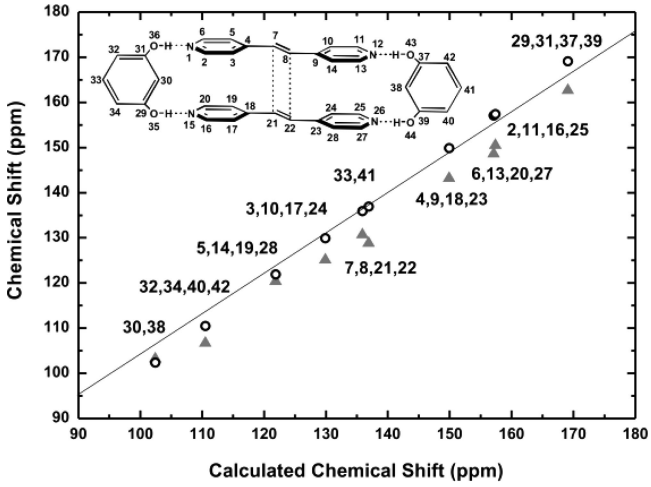

FIGURE 10. Plot of ^{13}C chemical shifts for the 1:1 co-crystallized *trans*-1,2-bis(4-pyridyl)ethylene (bpe) and resorcinol (2(bpe):2(res)). Open circles represent the computed, and triangles the experimentally observed ^{13}C chemical shifts with respect to the calculated values. (The solid line in the graph is a guide to eye.) The DFT computed ^{13}C shifts are based on an optimized 2(bpe):2(res) complex.

Figure 8 shows a series of ^{13}C CPMAS NMR spectra ranging from 1:1 co-crystallized 2(bpe):2(res) monomer prior to irradiation (0% conversion) to as-dimerized tetrakis(4-pyridyl)cyclobutane (triclinic $P\bar{1}$, 100% converted metastable phase), including partial mixture containing both monomer and dimer at ∼50% conversion (cf. Figure. 8b), whereas the spectrum in Figure 8d corresponds to another stable polymorph of tetrakis(4-pyridyl)cyclobutane with monoclinic $P2_1/n$ space group. As the dimerization proceeds, corresponding intensities of both the olefinic carbon (∼130 ppm) and ipso carbon signals (∼142 ppm) assigned to the monomer decreased with a gradual rise of the new carbon signals attributed to the cyclobutane ring, indicating successful formation of a photodimer. Additionally, the chemical shifts of the neighboring carbons, that is, the ipso (nonprotonated) carbon, display a small downfield shift upon conversion of the monomer into a dimer, possibly due to differences in inductive effects of neighboring groups (vinyl vs cyclobutane). Full assignments of the carbon sites in all samples are given in Table 1. Two signals in the cyclobutane ring region (∼40 ppm) and two signals in the resorcinol carbons (C4,C6) neighboring the resorcinol peripheral carbon (∼105 ppm) are observed in the respective ^{13}C CPMAS NMR spectra of both partially and fully converted as-dimerized metastable dimer (cf. Figure 8b,c). In contrast, the ^{13}C CPMAS NMR spectrum of 100% converted, stable recrystallized dimer complies with the ^{13}C solution NMR spectrum that exhibits a single peak in the respective regions reflecting the centrosymmetric molecular geometry.

New Polymorph of 2(bpe):2(res) Dimer. In homogeneous topochemical reactions, the overall volume change may be small, while changes of lattice parameters can be larger, for example, when van der Waals contacts are transformed into chemical bonds.[17] Notably, it has been observed while monitoring [2 + 2] photodimerization of monomer 2(bpe):2(res) via single-crystal X-ray analysis that the volume change during the transformation from monomer into dimer is less than 2%. However, even under tail irradiation conditions, crystals were observed to deteriorate, owing to an unusually large change of one angle in the unit cell (angle α), so that no single crystals of sufficient size were available for structure analysis at conversions exceeding approximately 50%. Nevertheless, powder diffractometry shows that $P\bar{1}$ phase (100% converted as-dimerized dimer) persists until complete conversion, which upon recrystallization adopted $P2_1/n$ phase (100% converted recrystallized dimer), which has already been reported.[16]

Notably, the ^{13}C CPMAS NMR spectra in Figure 8c,d provide evidence that the 100% converted as-dimerized and 100% converted recrystallized dimers are indeed two different polymorphs. Two different signals in the cyclobutane ring region in Figure 8c indicate that, though crystallographically the dimer is located on a center of symmetry, this is not reflected in the respective NMR spectrum due to its local environment (distortion of pyridyl rings as well as other packing effects) that exist in the as-dimerized dimer (triclinic, $P\bar{1}$ phase) resulting in signal splittings. In contrast, a single observed cyclobutane ring signal (∼40 ppm) hints at the absence of such molecular distortions so that the local symmetry center in the recrystallized dimer (monoclinic, $P2_1/n$ phase) is preserved. Even though ^{13}C chemical shifts of the $P\bar{1}$ polymorph of tetrakis(4-pyridyl)cyclobutane could not be computed due to lacking crystal structure coordinates (cf. Figure 11 caption), additional signals observed in the ^{13}C CPMAS spectrum of (Figure 8c) 100% converted as-dimerized dimer of 2(bpe):2(res) can be attributed to distortions in the structure caused by the tilt angle (i.e., the angle between the plane of the pyridyl ring and the bond connecting the pyridyl ring with cyclobutane ring) and strain developed during the SCSC transformation, thereby enforcing pyridyl rings to adopt different conformations. Figure 11 clearly reveals the different conformations of the pyridyl rings adopted in as-dimerized form and in recrystallized form.

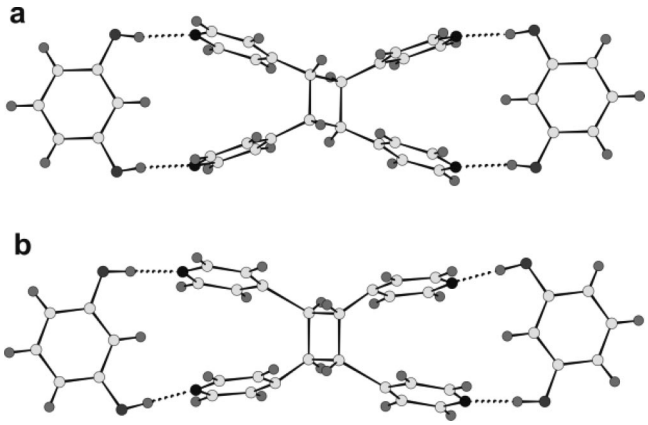

FIGURE 11. Crystal structure projections of the dimer molecules: (a) 100% converted recrystallized dimer with monoclinic $P2_1/n$ space group;[16] (b) 6 h irradiated (42% converted) as-dimerized dimer (as-irradiated product prior to recrystallization) with triclinic $P\bar{1}$ space group. From the latter structure, atoms belonging to the monomer have been removed for clarity (further details related to complete crystal structure analysis will be published elsewhere).[38]

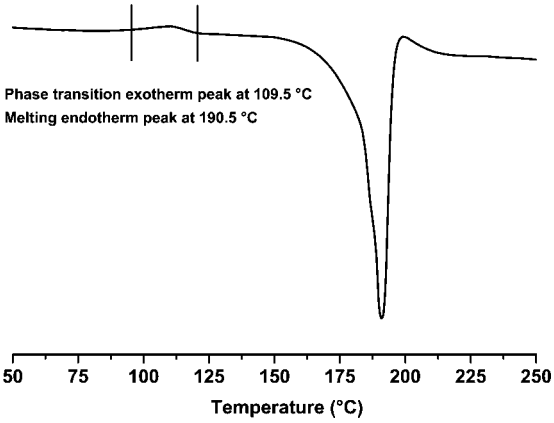

FIGURE 12. DSC plot for the 100% converted as-dimerized dimer of tetrakis(4-pyridyl)cyclobutane recorded at a heating rate of 10 °C/min. The melting temperature is ∼190 °C.

Thermal Analysis of 2(bpe):2(res) Dimer. Apparently, the as-dimerized form is in a metastable state;[40,41] that is, its as-dimerized conformation is not the equilibrium conformation. This results in lattice strain that facilitates adoption of a more stable conformation rather close to an equilibrium conformation similar to the one adopted by the recrystallized dimer. Consequently, a polymorphic phase transformation from the metastable $P\bar{1}$ phase to the more stable $P2_1/n$ phase of tetrakis(4-pyridyl)cyclobutane has been observed at ∼109 °C (DSC data, cf. Figure 12). However, the reverse transformation upon subsequent cooling is *not* observed. As can be seen in Figure 12, the DSC experiment provides clear evidence that the metastable $P\bar{1}$ phase transforms to the stable $P2_1/n$ phase, where an exotherm peak representing the phase transformation is observed at 109.5 °C, followed by melting at 190.5 °C (endotherm peak). A comparable exotherm peak is not observed in the DSC trace of 100% converted recrystallized dimer ($P2_1/n$ phase). Further evidence for the polymorphic transition stems from temperature-dependent solid-state ^{13}C NMR studies. First, the ^{13}C CPMAS NMR spectrum of 100% converted as-dimerized dimer was recorded at room temperature, yielding a spectrum similar to the one shown in Figure 8c. Then, the same compound was subjected to higher temperatures (up to ∼110 °C), where the obtained spectrum exhibited similar characteristics as shown in Figure 8d (explicitly, the two signals in the cyclobutane ring region have merged into one single signal) corresponding to the phase transition. A ^{13}C CPMAS spectrum of 100% converted as-dimerized dimer (triclinic, $P\bar{1}$) measured at a higher temperature (∼110 °C) is provided in Supporting Information.

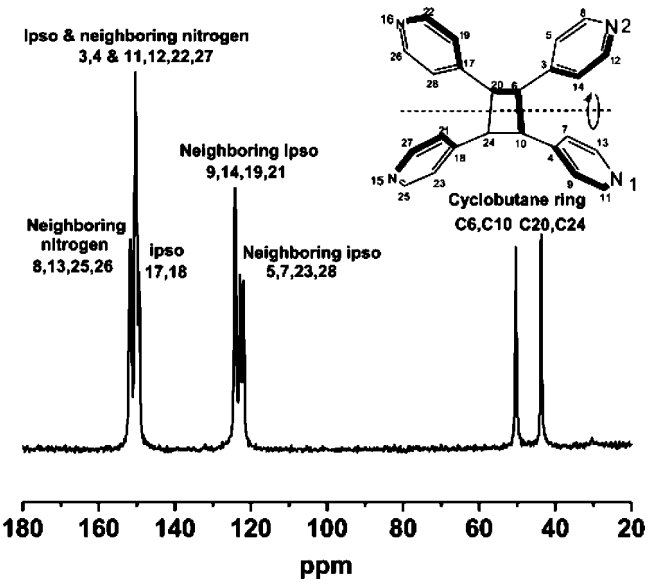

FIGURE 13. ^{13}C CPMAS NMR spectrum of pure extracted tetrakis(4-pyridyl)cyclobutane (1,2,3,4-tetra(pyridine-4-yl)cyclobutane). The presence of two signals in the cyclobutane ring region points toward the loss of the inversion center in the pure dimer.

Removal of Template from 2(bpe):2(res) Dimer. Finally, tetrakis(4-pyridyl)cyclobutane was separated by removal of resorcinol from the 2(bpe):2(res) recrystallized dimer complex ($P2_1/n$ phase) by column chromatography and recrystallized from acetone. Its purity was confirmed from both ^{1}H and ^{13}C solution NMR spectra (cf. Supporting Information) that displayed four different resonances, as expected for a centrosymmetric dimer. However, the solid-state ^{13}C CPMAS NMR spectrum exhibited more resonances than in solution; in particular, two different resonances were observed for the carbons (C6,C10,C20,C24) in the cyclobutane ring at ∼44 and ∼50 ppm (cf. Figure 13), hinting at a noncentrosymmetric structure as a consequence of possible distortions present in the crystal. The molecular packing of the compound is shown in Figure 14, which clearly reveals the distortion of the cyclobutane ring and also the presence of a 2-fold axis passing through the center of the cyclobutane ring of the molecule.

In comparison to both metastable as-dimerized dimer (triclinic, $P\bar{1}$ phase) and rather stable recrystallized dimer (monoclinic, $P2_1/n$ phase), tetrakis(4-pyridyl)cyclobutane crystallizes in an orthorhombic space group (*Pccn* (No. 56); $Z = 4$; with cell lengths of $a = 9.37$ Å, $b = 13.94$ Å, and $c = 14.05$ Å) with four molecules comprising the unit cell. Indeed, the crystal structure revealed a substantial distortion of the cyclobutane ring as a consequence of removing resorcinol. In the absence of hydrogen bonding, all pyridyl rings moved away from each other along with significant rotations attaining different conformations. Therefore, the cyclobutane ring no longer remained planar but

(40) Ahn, S.; Harris, K. D. M.; Kariuki, B. M.; Zin, D. M. S. *J. Solid State Chem.* **2001**, *156*, 10–15.
(41) Threlfall, T. L. *Analyst* **1995**, *120*, 2435–2460.

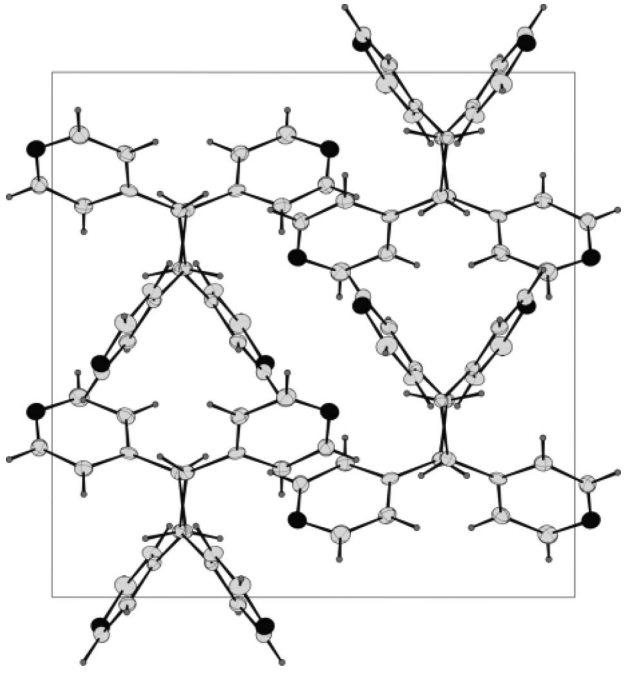

FIGURE 14. Molecular packing of pure extracted tetrakis(4-pyridyl)-cyclobutane (1,2,3,4-tetra(pyridine-4-yl)cyclobutane). The compound crystallizes in an orthorhombic lattice (space group *Pccn* (No. 56); $Z = 4$), where the tetrakis(4-pyridyl)cyclobutane moiety resides on a C_2-axis. Notably, the cyclobutane ring is not planar but rather puckered with all its hydrogen atoms slightly staggered, as previously observed for recrystallized truxillic acid.[18]

is puckered,[42] where all ring hydrogen atoms are slightly staggered as opposed to a totally eclipsed conformation adopted in the planar centrosymmetric ring of 2(bpe):2(res) dimer (Figure 11a).

The experimental ^{13}C CPMAS NMR data of tetrakis(4-pyridyl)cyclobutane were compared with DFT ^{13}C chemical shift computations based on an optimized geometry. The computed shifts revealed that all five carbons present in each pyridyl ring have different chemical shifts. However, the presence of a 2-fold axis passing through the center of cyclobutane ring has reduced the number of resonances to 12 instead of 24 as would be expected otherwise for all carbon atoms present in a single molecule. In contrast, the experimental ^{13}C CPMAS NMR spectrum (cf. Figure 13) exhibits only eight resonances as some of the chemical shift values are too similar to be resolved. Figure 15 shows the plot of computed ^{13}C isotropic chemical shifts versus the observed values; the agreement is good in the range of ±5 ppm.

3. Conclusions

Two different polymorphs of the monomer complex 2(bpe):2(res) have been obtained, a ring form ($P\bar{1}$, triclinic) that is suitable for photodimerization and a chain form ($P2_1/n$, monoclinic). In addition, two polymorphs of 2(bpet):2(res) have been found while exploring molecular specificity during resorcinol−pyridine recognition. Moreover, we have clearly demonstrated with the help of solid-state NMR analysis that the crystal-engineered monomer (ring form) complex of 2(bpe):2(res) also yielded two different dimer polymorphs upon photoirradiation

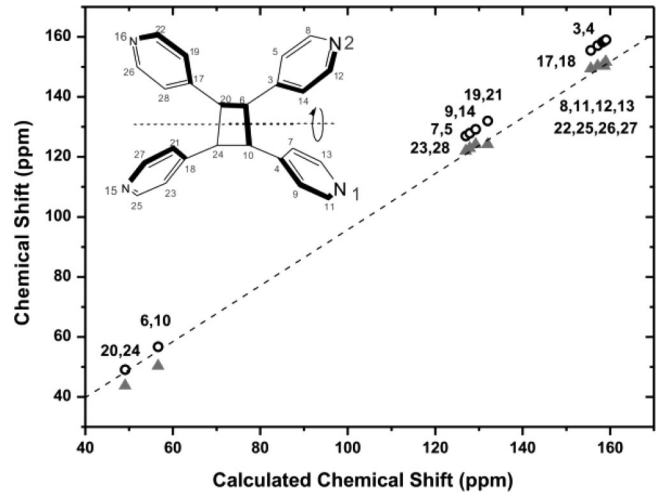

FIGURE 15. Plot of ^{13}C chemical shifts for tetrakis(4-pyridyl)cyclobutane (1,2,3,4-tetra(pyridine-4-yl)cyclobutane). Open circles represent the computed, and triangles the experimentally observed ^{13}C chemical shifts with respect to the calculated values (the solid line in the graph is a guide to eye). The computed ^{13}C shifts are based on a DFT optimized molecule, with a 2-fold axis passing through the center of the cyclobutane ring. Thus, the computation yielded 12 different chemical shifts that are symmetry-related to the other half of the molecule.

(e.g., the centrosymmetric (monoclinic, $P2_1/n$ phase, and triclinic, $P\bar{1}$ phase)). In addition, removal of the resorcinol template from the 2(bpe):2(res) complex yielded tetrakis(4-pyridyl)cyclobutane that consists of a distorted cyclobutane ring along with a rather different molecular geometry (orthorhombic, *Pccn* phase). Ambiguous peak splittings and the presence of "unexpected" resonances in the respective ^{13}C CPMAS NMR spectra have been successfully explained by the joint approach of X-ray analysis and DFT ^{13}C chemical shift computations. Since the computations are sensitive to intermolecular as well as solid-state packing effects, they yielded different chemical shifts for those atoms that are located in different environments (as extracted from the respective crystal structures).

4. Experimental Section

1,3-Dihydroxybenzene (resorcinol), *trans*-1,2-bis(4-pyridyl)ethylene (bpe), and 1,2-bis(4-pyridyl)ethane (bpet) are commercially available and were used as obtained. Co-crystals of 2(bpe):2(res) were prepared by dissolving 2 mmol of resorcinol (220.4 mg) and 2 mmol of bpe (364.6 mg) in 50 mL of acetone and left for slow evaporation in an open container. After 2 days, yellow crystals were obtained and subsequently ground to small microcrystalline particles. Five hundred milligrams of co-crystals was evenly distributed in a thin layer on a 100 mm Petri dish and irradiated using a 100 W high-pressure Hg lamp for a period of 12 h, yielding 100% converted as-dimerized tetrakis(4-pyridyl)cyclobutane (triclinic, $P\bar{1}$ phase). Aliquots of 125 mg product were taken out at each interval of 2 h for solid-state NMR measurements. In order to reach fast conversion, the powder was agitated after every 30 min and simultaneously rotated using a home-built small rotating machine. The 100% converted recrystallized dimer of tetrakis(4-pyridyl)cyclobutane (monoclinic, $P2_1/n$ phase) was obtained by recrystallization of as-dimerized bpe dimer from acetone.

Co-crystallization of *trans*-1,2-bis(4-pyridyl)ethylene (bpe) and 1,2-bis(4-pyridyl)ethane (bpet) with resorcinol in 0.5:0.5:1 ratio was performed by dissolving 0.5 mmol of bpe (91.15 mg), 0.5 mmol of bpet (92.15 mg), and 1 mmol of resorcinol (110.2 mg) in 25 mL of acetone and left for slow evaporation in an open container. After ∼48 h, different kinds of crystals were obtained; yellow

(42) Henseler, D.; Hohlneicher, G. *J. Phys. Chem. A* **1998**, *102*, 10828–10833.

crystals were formed at the bottom of the container, whereas colorless crystals were found on the walls. Yellow crystals were then first subjected to X-ray analysis and found to be co-crystals of a new polymorph (polymorph **2**) of 2(bpe):2(res) in chain conformation (monoclinic, $P2_1/n$), whereas the colorless crystals were identified as co-crystals of 2(bpet):2(res) also in the chain form with almost identical lattice parameters with those of chain 2(bpe):2(res).

Extraction of Tetrakis(4-pyridyl)cyclobutane from 2(bpe):2(res) Dimer Complex: 1,2,3,4-Tetra(pyridine-4-yl)cyclobutane was separated from 200 mg of dimerized co-crystals (monoclinic, $P2_1/n$ phase) of 2(bpe):2(res) via column chromatography using acetone. Resorcinol eluted first, followed by 1,2,3,4-tetra(pyridine-4-yl)cyclobutane. Subsequent evaporation of solvents yielded a yellowly powder of 1,2,3,4-tetra(pyridine-4-yl)cyclobutane (orthorhombic, *Pccn* phase). Single crystals for X-ray analysis were obtained by slow evaporation of an acetone solution: ^{1}H NMR δ 8.71−8.69 (d, 8H, N-CH), 7.26−7.24 (d, 8H, N-CH-CH), 4.73 (s, 4H, cyclobutane ring); ^{13}C NMR δ 150.43 (8C, N−C), 149.2 (4C, ipso), 124.1 (8C, next to ipso), 46.2 (4C, cyclobutane ring); EIMS m/z 363.6 (M^+).

Solid-State NMR: All ^{13}C CPMAS spectra were collected at 125.77 MHz with a CP contact time of 5 ms coadding 8196 transients. The experiments were carried out using a standard 4 mm double resonance MAS probe spinning at 12 kHz, typical $\pi/2$-pulse length of 2.5 μs, and a recycle delay of 15 s. The spectra are referenced with respect to tetramethyl silane (TMS) using adamantane as secondary standard (29.46 ppm for ^{13}C).[43] If not stated otherwise, all spectra were acquired at room temperature.

Solution NMR and Mass: Solution ^{1}H NMR spectra were recorded at 250.1 MHz. The residual ^{1}H peak of the deuterated solvent was used as an internal standard (acetone, ^{1}H, $\delta = 2.05$ ppm). Mass spectra were obtained at 70 eV.

DFT-Based Chemical Shift Calculations: Geometries were taken from the respective crystal structures and optimized (where appropriate) at the BLYP/6-311G(2df,2pd) level of theory.[44,45] Relaxing the structures during a geometry optimization may yield C−H bond lengths that differ up to 0.15 Å from the initial structure while keeping the heavy atoms almost unchanged.[46] This, however, is *not* feasible for as-dimerized (that is, as-irradiated product prior to recrystallization) and intermediate states that both are rather metastable structures. While full consideration of crystal packing effects (e.g., structure optimization using periodic boundaries[46]) is indeed crucial for an accurate prediction of ^{1}H chemical shifts (e.g., ±1 ppm or better, with a typical ^{1}H chemical shift range of 20 ppm), this is less critical for ^{13}C chemical shifts. In fact, the ^{13}C chemical shift range of 200 ppm renders the average deviation of computed ^{13}C chemical shifts (using DFT optimized molecular structures) of about ±5−6 ppm fairly good. All DFT ^{13}C chemical shifts were referenced with respect to tetramethylsilane (TMS) and computed at B3LYP/6-311++G(2df, 2pd) or B3LYP/6-311G(2df,2pd) level of theory[44,45] with the GIAO approach as implemented in Gaussian03 program package.[47]

Single-Crystal X-ray Analysis: X-ray structures were recorded on a Kccd diffractometer with graphite-monochromated Mo Kα radiation. Lattice parameters were obtained by least-squares fits to the scattering angles of reflections observed in several prescans. The intensity data collection was performed by ϕ and ω scans; all raw data were corrected for Lorentz and polarization effects. The structures were solved by direct methods and refined by full matrix least-squares analyses with anisotropic temperature factors for all atoms except protons. Proton positions were calculated using known molecular geometries, refined in riding mode with fixed isotropic temperature factors. Empirical absorption corrections were applied to the data.

Supporting Information Available: Crystal structures of tetrakis(4-pyridyl)cyclobutane, polymorph **2** of 2(bpe):2(res), and polymorph **2** of 2(bpet):2(res) are provided as cif files. Furthermore, solution ^{13}C NMR spectra of resorcinol, *trans*-1,2-bis(4-pyridyl)ethylene (bpe), 2(bpe):2(res) monomer (ring form, $P\bar{1}$ phase), recrystallized 2(bpe):2(res) dimer ($P2_1/n$ phase), tetrakis(4-pyridyl)cyclobutane, the solid-state ^{13}C CP-MAS NMR spectrum of as-dimerized 2(bpe):2(res) dimer ($P\bar{1}$ phase) at 110 °C, as well as the solution ^{1}H NMR spectrum of both 2(bpe):2(res) monomer (chain form) and 2(bpet):2(res) monomer (chain form) are given. In addition, all *xyz* coordinates obtained from the respective DFT structure optimizations are available. This material is available free of charge via the Internet at http://pubs.acs.org.

JO802673F

(43) Morkombe, C. R.; Zilm, K. *J. Magn. Reson.* **2003**, *162*, 479–486.
(44) Becke, A. D. *Phys. Rev.* **1988**, *38*, 3098–3100. (b) Lee, C.; Yang, W.; Parr, R. G. *Phys. Rev.* **1988**, *A37*, 785–789.
(45) Krishnan, R.; Binkley, J. S.; Seger, R.; Pople, J. A. *J. Chem. Phys.* **1980**, *72*, 650–654.
(46) Schmidt, J.; Hoffmann, A.; Spiess, H. W.; Sebastiani, D. *J. Phys. Chem. B* **2006**, *110*, 23204–23210.
(47) Frisch, M. J. *Gaussian 03*, revision D.02; Gaussian, Inc.: Wallingford, CT, 2004. The complete reference is available in the Supporting Information.